Flexible Meandered UHF RFID Tag Antenna on Oiled-Paper: Impact of Chip Placement and Material Proximity for Industrial Applications

Hamza Othmani *, Jamel Smida, Mohamed Karim Azizi

Posted Date: 17 March 2026

doi: 10.20944/preprints202603.1222.v1

Keywords: UHF RFID; tag antenna; meandered dipole; chip placement; miniaturization; material proximity; industrial applications

 doi:10.20944/preprints202603.1222.v1

Article

Flexible Meandered UHF RFID Tag Antenna on Oiled-Paper: Impact of Chip Placement and Material Proximity for Industrial Applications

Hamza Othmani [1,*], Jamel Smida [1,2] and Mohamed Karim Azizi [1,3]

[1] Microwave Electronics Research Laboratory, Faculty of Sciences of Tunis, University of Tunis El Manar, 2092 Tunis, Tunisia
[2] College of Applied Science, AlMaarefa University, Riyadh 11597, Saudi Arabia
[3] Microwave Electronics Research Laboratory, Higher Institute of Arts and Multimedia, University of Manouba, 2010 Manouba, Tunisia
* Correspondence: hamza.othmani@fst.utm.tn

Abstract

In this work, the design and experimental validation of passive UHF RFID tag antennas are presented with the objective of evaluating the impact of chip placement and miniaturization approaches on tag performance. Four initial antenna layouts were developed by varying the position of the RFID integrated circuit within a coupling loop. Simulations and measurements confirmed that Antenna 1 achieved the best impedance matching, with a minimum reflection coefficient of −40 dB at 866 MHz and a power sensitivity of −16.3 dBm. Based on this reference design, a miniaturized version (Antenna 5) was obtained by integrating meander lines and capacitive end-loading, reducing the physical size while maintaining resonance at 866 MHz. Both structures were fabricated and evaluated using a Voyantic Tagformance measurement system, with read-range measurements performed under free-space conditions and in proximity to dielectric and metallic materials. The results demonstrated a maximum read range of 8.6 m for Antenna 1 in free space, while Antenna 5 preserved a read range of 6.3 m. In the presence of copper, Antenna 1 maintained a read range of 3 m, whereas Antenna 5 achieved approximately 0.5 m, confirming the robustness of the proposed designs in representative industrial environments.

Keywords: UHF RFID; tag antenna; meandered dipole; chip placement; miniaturization; material proximity; industrial applications

1. Introduction

Radio Frequency Identification (RFID) has become a key enabling technology in modern information and communication systems, supporting a wide spectrum of applications that require efficient, reliable, and contactless identification. In supply chain management [1], RFID enables real-time traceability and inventory optimization, while in healthcare it enhances patient safety [2–5], pharmaceutical monitoring [6], and medical equipment tracking [7,8]. In industrial automation, RFID contributes to intelligent production flows, asset monitoring, and predictive maintenance strategies [9,10]. Moreover, RFID-based access control systems ensure secure authentication in transportation networks and service infrastructures [11,12]. Beyond these application-specific contexts, RFID plays a central role in digital transformation frameworks by enabling robust object identification and seamless data integration within cyber–physical systems [13,14].

An RFID system typically consists of a reader equipped with a dedicated antenna and a tag integrating both an antenna and an integrated circuit (IC). Depending on their powering mechanism, RFID tags are classified as passive, semi-passive, or active. Passive tags operate exclusively by harvesting energy from the incident electromagnetic field, semi-passive tags incorporate a small battery to support internal circuitry, and active tags rely on an internal power source for communication and

 doi:10.20944/preprints202603.1222.v1

sensing functionalities [15]. RFID technology spans several frequency bands, including Low Frequency (LF, 125–134 kHz), High Frequency (HF, 13.56 MHz), and Ultra-High Frequency (UHF, 860–960 MHz), which supports long-range identification and high data-rate operation [16]. Among these, the UHF band has emerged as the dominant choice for large-scale logistics and industrial deployments due to its extended read range, rapid inventory capability, and compatibility with global supply-chain standards [17,18].

Despite its widespread adoption, the design of UHF RFID tag antennas continues to face several unresolved challenges. One of the most critical issues is achieving reliable conjugate impedance matching between the antenna and the highly capacitive RFID IC, as any mismatch directly degrades power transfer efficiency and limits the achievable read range [19,20]. In addition, antenna sensitivity remains a limiting factor, particularly in industrial environments where tags are exposed to diverse surrounding materials that significantly alter their electromagnetic behavior [21,22]. Proximity to dielectric or metallic objects often results in resonance detuning, bandwidth reduction, and severe radiation efficiency degradation [23,24]. Environmental conditions such as humidity, temperature variations, and mechanical stress further complicate tag operation and impose additional constraints on long-term reliability and robustness [25,26].

Another major design challenge lies in antenna miniaturization. Compact tag antennas are highly desirable for integration into modern packaging, wearable platforms, and embedded sensing systems [27–30]. However, reducing the antenna footprint typically leads to increased losses, narrower bandwidth, and greater sensitivity to material loading effects [31]. To address these issues, various miniaturization strategies have been explored, including meander-line geometries, folded dipole structures, and capacitive loading techniques [32–34]. While these approaches enable size reduction, they often introduce trade-offs between efficiency, bandwidth, robustness, and manufacturability, particularly when flexible or unconventional substrates are considered [35].

In this context, the development of flexible UHF RFID tag antennas capable of maintaining stable performance under material proximity and industrial constraints remains an open research problem. Substrate selection plays a crucial role in this regard, as unconventional and low-cost materials may offer advantages in terms of flexibility and sustainability but may also introduce additional electromagnetic uncertainties. Furthermore, chip placement tolerance and robustness against environmental loading are rarely addressed jointly in existing studies, despite their practical relevance for large-scale industrial deployments [36,37].

This paper presents the design of a flexible meandered UHF RFID tag antenna fabricated on an oiled-paper substrate, with a particular focus on robustness and practical deployment constraints. An experimental investigation is conducted to evaluate the tolerance of the antenna to variations in RFID chip placement and to analyze the impact of such variations on impedance matching and read-range stability. The robustness of the proposed design is further examined under proximity to industrially relevant materials, including metallic surfaces. The performance of the proposed antenna is comparatively assessed against state-of-the-art UHF RFID tag antennas in terms of physical size, operational bandwidth, and achievable read range. In addition, an experimental benchmark against two commercially available UHF RFID tags is performed under identical free-space and material-proximity conditions, providing a realistic reference for evaluating read-range degradation trends and overall robustness in representative industrial scenarios.

The remainder of this paper is organized as follows. Section 2 introduces the theoretical background and equivalent circuit modeling. Section 3 presents the antenna configurations and experimental validation. The measured and simulated results are then discussed, followed by concluding remarks.

 doi:10.20944/preprints202603.1222.v1

2. Antenna Design and Theoretical Background

2.1. Antenna Geometry and Operating Band

The proposed UHF RFID tag is implemented as a meandered dipole structure on a flexible oiled-paper substrate ($\varepsilon_r = 3.87$, thickness $= 0.2$ mm), with the radiating element fabricated in copper (thickness $= 0.035$ mm). The design operates within the UHF RFID band of 865–868 MHz, with a nominal resonance at 866.6 MHz. The initial layout is derived from a half-wavelength dipole optimized for the UHF range and is shortened through meander sections to reduce the physical length while maintaining the required electrical path.

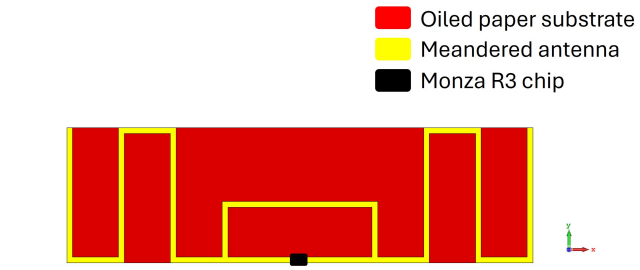

Figure 1. Proposed meandered UHF RFID tag design.

In this study, four reference configurations were realized, differing only in the placement of the IC along the dipole loop region, in order to provide a systematic evaluation of chip-location effects on input impedance and matching.

2.2. Electrical Model of the RFID Tag

The equivalent circuit of an RFID tag is shown in Figure 2. The source V_a corresponds to the open-circuit RF voltage at the antenna terminals. The impedance of the chip reflects both its input properties and the parasitic elements of the package. Both Z_a and Z_{chip} vary with frequency, and Z_{chip} may also depend on the incident power level. For proper operation, the antenna is designed to achieve conjugate matching with the chip at the minimum activation power.

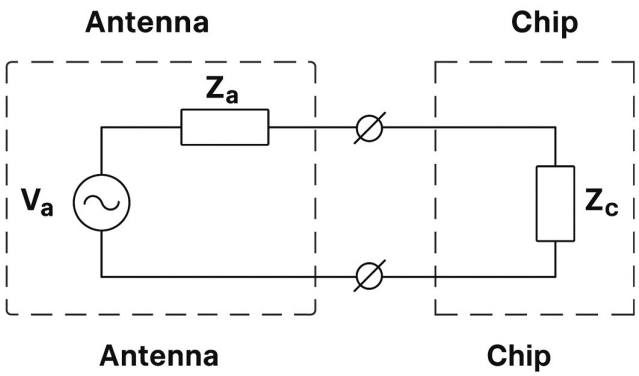

Figure 2. Equivalent circuit representation of the RFID tag.

The antenna is modeled by its complex impedance

$$Z_a = R_a + jX_a \tag{1}$$

The chip is represented by

$$Z_{chip} = R_{chip} - jX_{chip} \tag{2}$$

 doi:10.20944/preprints202603.1222.v1

The design objective is to satisfy the conjugate-matching condition at the nominal frequency f_0

$$Z_a = Z_{chip}^* \tag{3}$$

which maximizes the power delivered to the chip and represents the standard design criterion in the development of UHF RFID tags.

2.3. Electrical Modeling of the RFID Chip

The RFID integrated circuit (IC) is a fundamental component in the operation of the UHF tag, as it defines the conditions for energy transfer from the reader and backscatter data communication. In this study, the Impinj Monza R3 IC is selected, a widely used chip compliant with EPC Gen2 technology and recognized for its stable performance. Its input impedance is $Z_{chip} = 32 - j228\,\Omega$ [38], making conjugate matching with the antenna impedance essential to maximize power transfer and ensure reliable tag activation.

Although it belongs to an older generation, the Monza R3 chip remains practical for laboratory prototyping due to its quad-pad configuration (RF1, RF2, GND, GND), which allows straightforward manual soldering without specialized equipment. More recent chips, such as the Monza R6, are significantly smaller and generally require dedicated packaging modules (e.g., from Murata), which increases fabrication cost. The Monza R3 exhibits a read sensitivity of approximately -15 dBm, compared to about -22 dBm for the Monza R6. Despite this limitation, the experimental results obtained in this study remain satisfactory.

For accurate impedance matching during antenna design, the chip is represented by an equivalent circuit implemented in CST Studio Suite. In this work, the chip is modeled using a series configuration, where the real part is represented by a resistance (R_s) and the reactive part by a capacitance (C_s). In the simulation environment, discrete ports define the resistive value in ohms, while lumped elements represent the capacitive component in farads, as illustrated in Figure 3.

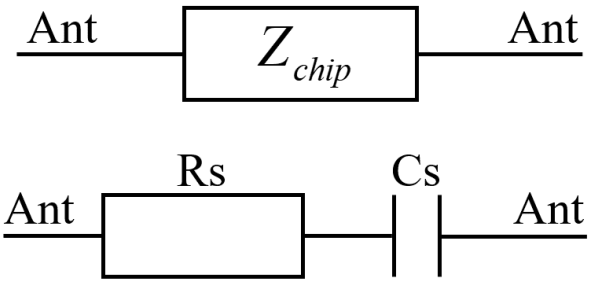

Figure 3. Equivalent circuit configuration of the RFID chip.

This equivalent circuit provides a reliable representation of the chip behavior and its interaction with the antenna. The resistance and capacitance values are derived directly from the complex chip impedance and are then used to optimize the matching performance at the resonance frequency f_0:

$$Z_{chip} = R_{chip} - jX_{chip} \tag{4}$$

According to the equivalent series model shown in Figure 2, the chip impedance defined in Eq. (2) can also be expressed in terms of R_s and C_s as

$$R_s = R_{chip} \tag{5}$$

$$C_s = \frac{1}{2\pi f_0 X_{chip}} \tag{6}$$

 doi:10.20944/preprints202603.1222.v1

3. Analysis of the Reference Antenna Configurations

3.1. Description of Antenna Configurations

As illustrated in Figure 4, four configurations of the Monza R3 IC placement on the meandered dipole tag were investigated. In Configuration 1, the IC is mounted at the central position of the loop, aligned with the lower edge of the structure. In Configuration 2, the IC is placed at the upper edge of the loop with a vertical offset of W_1. In Configuration 3, the loop is separated from the dipole arms by a gap of $a = 1$ mm, and the IC is positioned on the inner side of the loop.

In Configuration 4, the loop antenna gap is extended to $b = 3$ mm, and the IC is located at the upper part of the loop. In Configurations 1 and 2, the IC is directly connected to the loop, whereas Configurations 3 and 4 introduce a controlled separation between the coupling loop and the radiating arms. This approach enables a comparative evaluation between direct mounting and loop-gap integration.

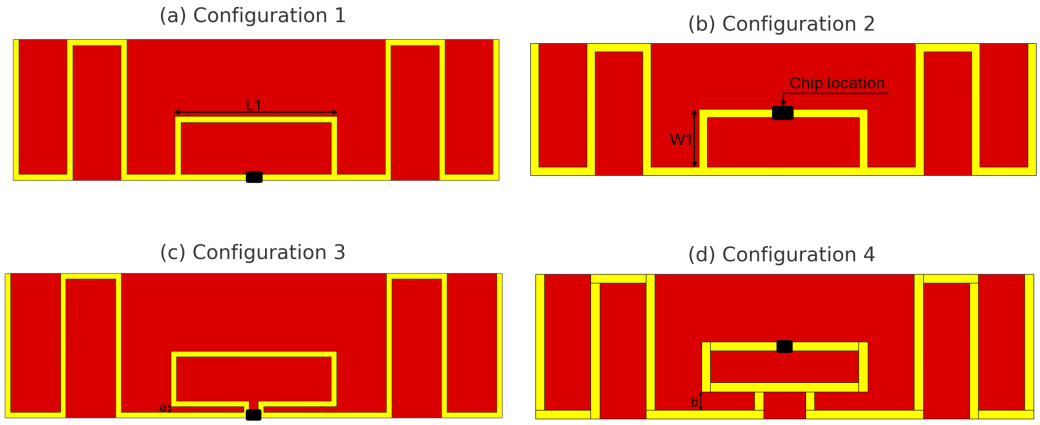

Figure 4. Different design layouts of the meandered UHF RFID tag (Configurations 1–4).

Modifying the IC position within the tag structure is not merely a geometrical displacement. Each configuration required specific adjustments to the antenna dimensions (length and width) in order to preserve impedance matching. This fine-tuning ensured that all variants operate within the European UHF RFID band, maintaining resonance at $f_0 = 866.6$ MHz.

3.2. Simulation and Measurement Setup

The four antenna configurations were modeled in CST Studio Suite and optimized to resonate at $f_0 = 866.6$ MHz. Figure 5 presents the simulated reflection coefficients (S_{11}) for the different structures. Small frequency shifts are observed due to variations in the IC location, which directly influence the impedance matching between the antenna and the chip. The geometrical parameters were iteratively refined to ensure that all structures resonate within the designated frequency band.

Antennas 1 and 2 exhibit excellent impedance matching, with minimum return-loss values of approximately -40 dB and -45 dB, respectively. These results confirm the effectiveness of directly mounting the RFID IC within the coupling loop, enabling strong conjugate interaction at resonance. Antenna 3 presents a moderate response, with a return-loss minimum around -20 dB, indicating reduced matching efficiency but still acceptable performance. Antenna 4 represents the least efficient configuration, with a minimum near -17 dB. Although this value remains below the conventional -10 dB matching threshold, the adaptation is significantly weaker compared to the first two configurations. The progressive degradation observed from Antennas 1–2 to Antennas 3–4 results from the increased separation between the coupling loop and radiating arms ($a = 1$ mm and $b = 3$ mm), which weakens the electromagnetic coupling.

 doi:10.20944/preprints202603.1222.v1

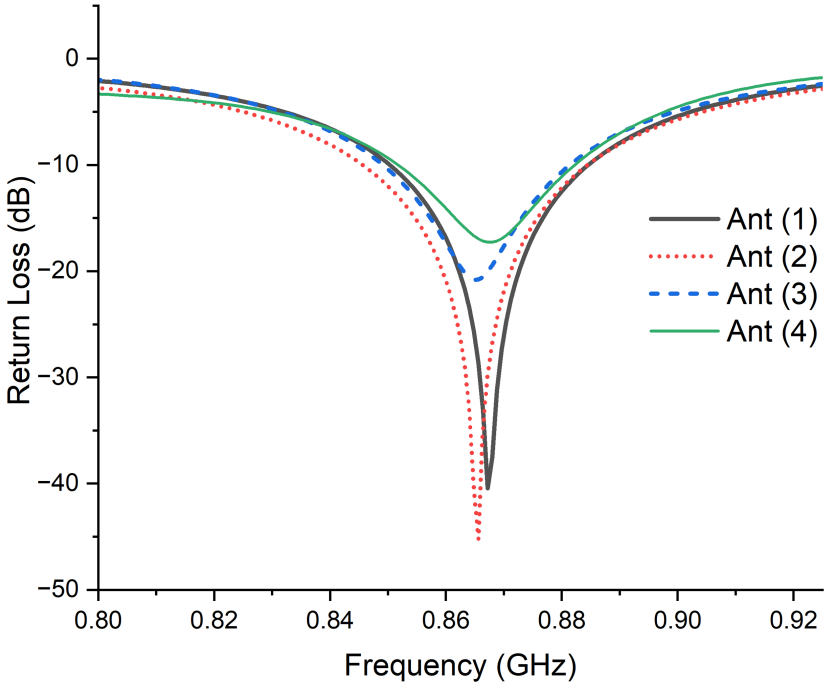

Figure 5. Return-loss characteristics of Antennas 1–4 in the UHF band.

3.3. Power Sensitivity Evaluation

Experimental Setup:

While reflection coefficients provide an initial indication of impedance matching quality, the practical performance of UHF RFID tags must also be evaluated in terms of the minimum power required to activate the IC, commonly referred to as *power sensitivity*. This parameter was measured using an M6E evaluation board equipped with an RF front-end and connected via a coaxial cable to a reader antenna. The board was interfaced with a computer that controlled the measurement procedure and recorded the data.

During testing, the fabricated tag antennas were positioned approximately 1 m from the reader antenna. The system recorded the minimum transmitted power at which each tag was successfully energized, providing a direct measure of power sensitivity, as shown in Figure 6.

Impact of IC Placement on Tag Sensitivity:

The power sensitivity measurements provide a clear comparison among the four configurations. Antenna 1 exhibited the lowest required input power, with a minimum of −16.3 dBm at 866 MHz, confirming the advantage of placing the IC directly within the coupling loop to ensure strong conjugate impedance interaction. Antenna 2 showed nearly identical performance, with a minimum of −16.2 dBm. Antenna 3 required approximately −15.2 dBm, indicating reduced sensitivity due to partial decoupling caused by the increased loop offset. Antenna 4 demonstrated the weakest performance, with a minimum of −14.7 dBm, corresponding to a noticeable degradation in power transfer efficiency.

These results demonstrate that IC placement within the radiating structure not only affects the reflection characteristics but also directly influences tag sensitivity and the practical read range. The spatial relationship between the coupling loop and the antenna arms governs the impedance transformation efficiency, determining how effectively the IC can be energized under low-power conditions. Therefore, precise IC positioning is a critical design parameter in UHF RFID tag optimization.

 doi:10.20944/preprints202603.1222.v1

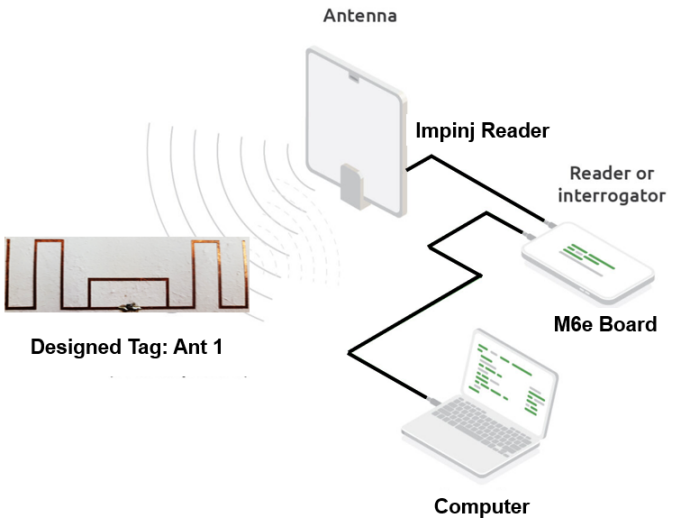

Figure 6. Experimental setup for sensitivity measurement of the designed RFID tags.

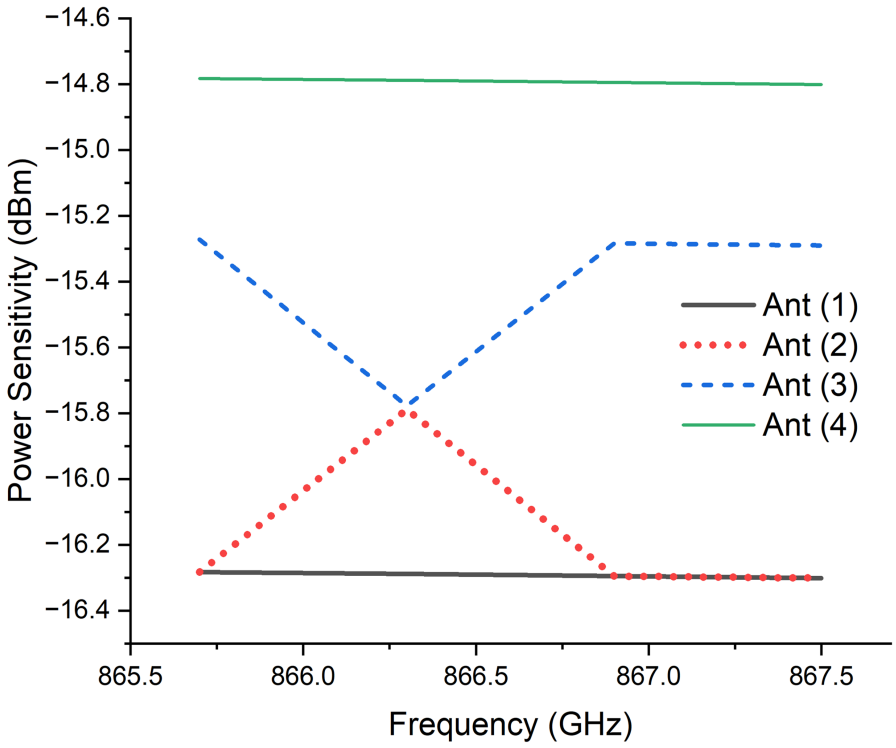

Figure 7. Power sensitivity of the four RFID tag antenna configurations.

4. Miniaturized Antenna Design and Robustness Evaluation

4.1. Miniaturized Antenna: Antenna 5

Based on the comparative analysis of the four reference configurations, Antenna 1 was identified as the most efficient structure and selected as the reference model for miniaturization. In this stage, additional meandered sections were introduced into the radiating arms in order to reduce the physical size while preserving the effective electrical length.

The incorporation of these folded lines initially shifted the resonance toward higher frequencies due to modifications in the current distribution. This shift was compensated through iterative adjustments of the meander lengths and trace widths, restoring resonance at 866 MHz.

To further enhance impedance matching, a capacitive end-loading was implemented at the extremities of the structure. This technique improves reactive compensation and facilitates conjugate matching between the antenna input impedance and the RFID chip while maintaining compact dimensions.

 doi:10.20944/preprints202603.1222.v1

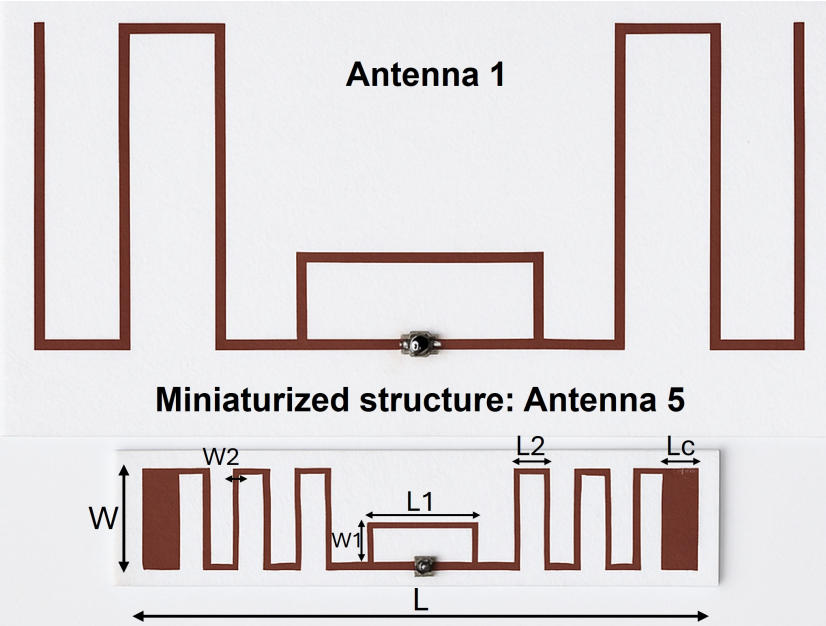

Figure 8. Design parameters of Antenna 1 and the miniaturized Antenna 5.

The optimized geometric parameters of the miniaturized antenna (Antenna 5) are summarized in Table 1. These values correspond to the final configuration obtained after integrating the meandered sections and capacitive end-loading, ensuring resonance at 866 MHz within the European UHF RFID band.

Table 1. Optimized design parameters of the meandered dipole antenna (Antenna 5).

Description	Parameter	Value (mm)
Antenna length	L	68.9
Antenna width	W	12.5
Loop length	L_1	11.0
Loop width	W_1	5.0
Meandering length	L_2	4.15
Capacitive loading length	L_c	3.2
Trace width	W_2	0.58
Substrate thickness	–	0.2
Copper thickness	–	0.035

4.2. Material Proximity Effects

Measurement Setup Using Voyantic Tagformance:

The performance of the fabricated tags was evaluated using the Voyantic Tagformance measurement system, a widely adopted platform for RFID characterization. The setup consists of a calibrated reader antenna and a controlled measurement station that excites the tag under test. The reader antenna was positioned at a fixed distance of 30 cm from the fabricated tag. A low-loss spacer ($\varepsilon_r \approx 1$) was used to maintain quasi-free-space conditions.

The Tagformance software enables accurate extraction of key parameters, including transmitted power, backscattered power, radar cross section (RCS), theoretical read range, and orientation sensitivity across the UHF RFID band.

 doi:10.20944/preprints202603.1222.v1

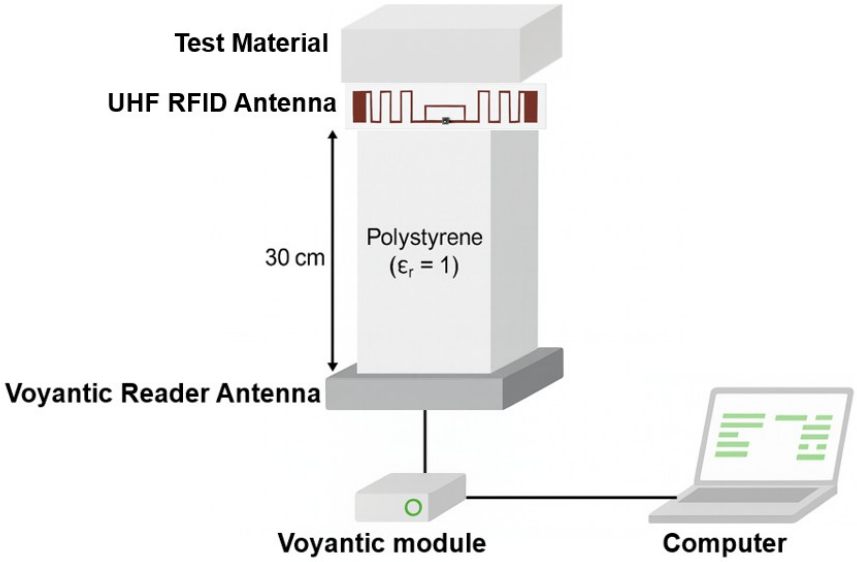

Figure 9. Measurement setup for the UHF RFID antenna in proximity to test materials.

Read Range Evaluation of Antenna 1:

The objective of this experiment was to evaluate tag performance in proximity to different materials representative of practical industrial environments. Figure 11 presents the measured forward read range of Antenna 1 under various loading conditions.

In the reference configuration, the antenna was placed on a polystyrene support at a fixed distance of 30 cm from the reader antenna. Under these quasi-free-space conditions, Antenna 1 achieved a maximum read range of approximately 8.6 m at 866 MHz.

When a wooden plate ($20 \times 20\,cm^2$) with a thickness of 9 mm was placed above the tag, the read range decreased to approximately 5 m. Increasing the wood thickness to 15 mm further reduced the read range to about 4 m.

For metallic loading, a copper sheet was introduced. To prevent electrical short-circuiting, a 5 mm polystyrene spacer was inserted between the tag and the metallic surface, as illustrated in Figure 10.

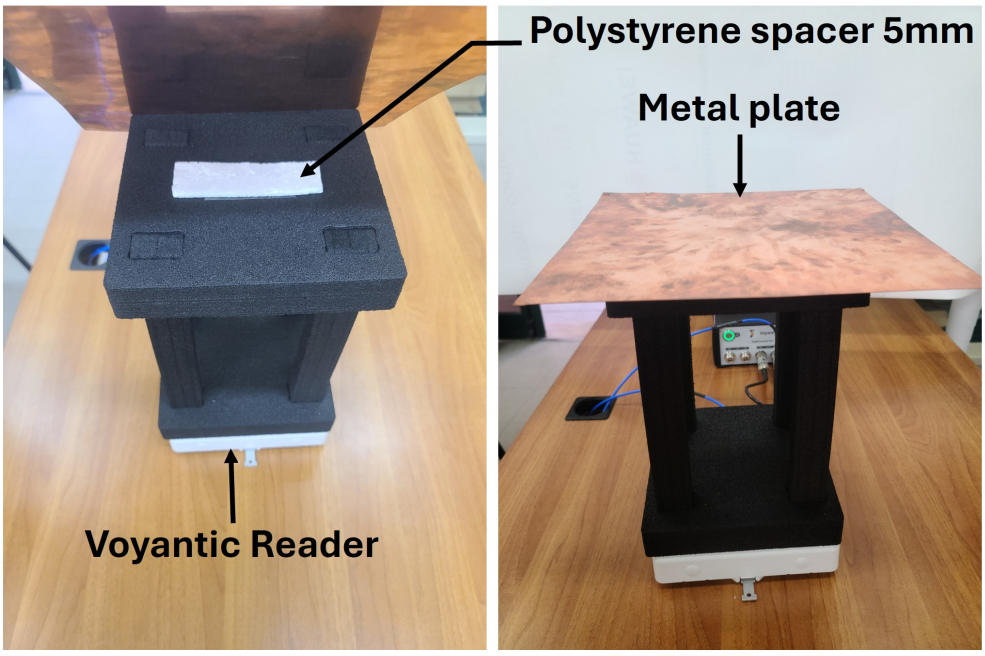

Figure 10. Experimental setup for RFID antenna measurement with spacer and material plate.

 doi:10.20944/preprints202603.1222.v1

Under metallic proximity, the antenna performance degraded further, with the read range limited to approximately 3 m. Increasing the copper thickness to 0.5 mm produced a similar effect, maintaining a read range close to 3 m at 866 MHz.

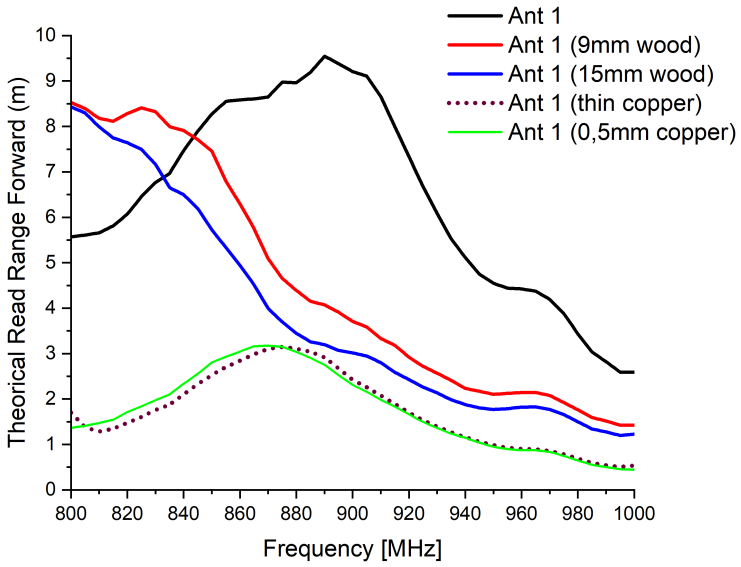

Figure 11. Theoretical read range of Antenna 1 under different material loading conditions.

Read Range Evaluation of Antenna 5:

For the miniaturized structure (Antenna 5), a noticeable reduction in performance was observed compared to Antenna 1. Under free-space conditions, the maximum forward read range reached approximately 6.3 m at 866 MHz.

When loaded with a 9 mm wooden plate, the read range decreased significantly to about 1.6 m and further dropped to approximately 1.3 m with a 15 mm wooden plate.

In the presence of copper layers, regardless of thickness (thin sheet or 0.5 mm), the read range was severely limited, stabilizing around 0.5 m.

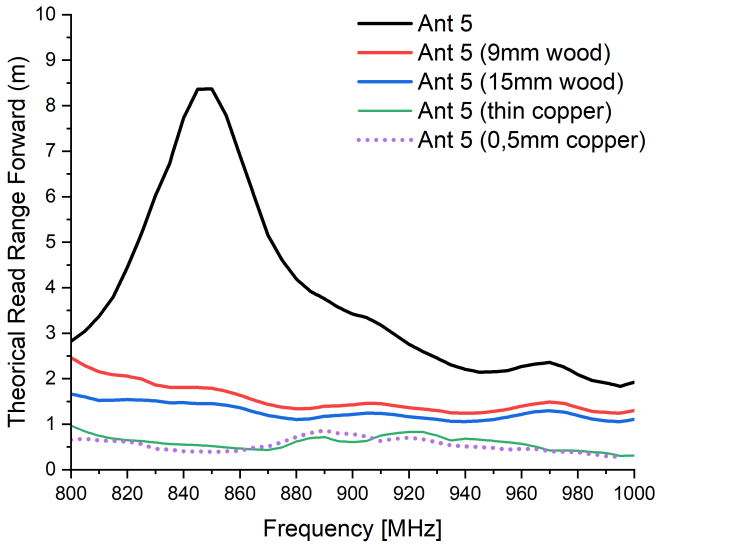

Figure 12. Theoretical read range of Antenna 5 under different material loading conditions.

 doi:10.20944/preprints202603.1222.v1

Normalized Radiation Patterns:

Figure 13 presents the normalized radiation patterns (in dB) of the two most efficient structures: Antenna 1 and its miniaturized version, Antenna 5. Despite the dimensional reduction and the decrease in free-space read range, both antennas preserve a similar angular distribution, characterized by a bidirectional pattern with main lobes oriented at 0° and 180°.

This result indicates that the miniaturization process did not significantly alter the fundamental radiation characteristics of the dipole-based structure, thereby maintaining acceptable orientation stability and spatial coverage.

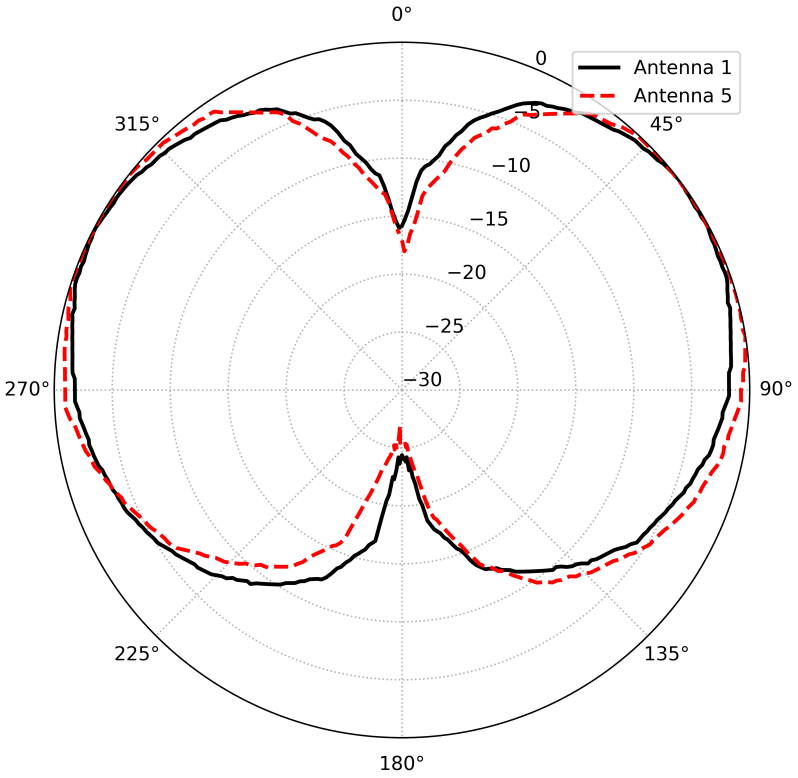

Figure 13. Normalized radiation patterns of Antenna 1 and Antenna 5.

4.3. Commercial Tag Benchmark

To contextualize the material-proximity results obtained for the proposed antennas, additional measurements were conducted on two commercially available UHF RFID tags used as practical benchmarks. This comparison provides a reference level of read-range degradation under dielectric and conductive loading conditions.

Figure 14 presents the measured read range versus frequency for two commercial UHF RFID tags under three conditions: free space, wood proximity, and copper proximity.

The first benchmark, a commercial tag equipped with an NXP UCODE 8 integrated circuit, exhibits a maximum read range of approximately 6.5 m at 866.6 MHz under free-space conditions. When a wooden slab is placed in direct proximity, the read range decreases to about 5 m, corresponding to a reduction of nearly 23%. In the presence of copper, a more significant degradation is observed, with the read range reduced to approximately 2.5 m, representing a reduction exceeding 60% relative to free space.

The second benchmark, a ThinPropeller 2006 commercial tag equipped with an Alien Higgs-2 IC, achieves a free-space read range of approximately 7.2 m at 866.6 MHz. Under wood proximity, the read range decreases to about 5.5 m. In the presence of copper, a pronounced degradation occurs, limiting the maximum read range to approximately 1.9 m.

 doi:10.20944/preprints202603.1222.v1

These results highlight the strong sensitivity of commercially available RFID tags to nearby materials, particularly conductive objects, despite being optimized for logistics and tracking applications.

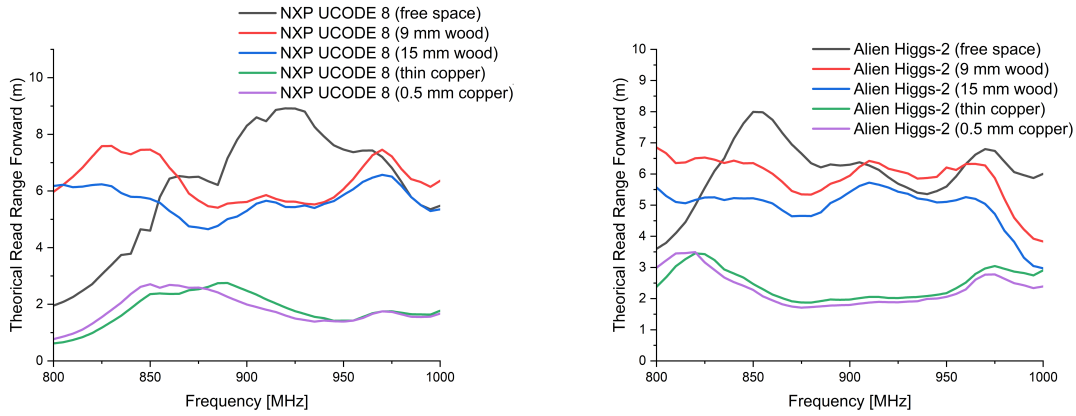

Figure 14. Measured read range versus frequency for two commercially available UHF RFID tags under free-space conditions and in proximity to wood and copper. Left: Commercial tag B (NXP UCODE 8). Right: Commercial tag A (ThinPropeller 2006, Alien Higgs-2).

Table 2 summarizes the measured read range values and the corresponding degradation induced by wood and copper proximity for the proposed antennas and the commercial benchmarks, under identical experimental conditions at 866.6 MHz.

Table 2. Comparative read range performance of the proposed tag antennas and commercially available RFID tags under different material proximity conditions at 866.6 MHz.

Tag / Antenna	IC	Free-space (m)	Wood (m)	Copper (m)	Degradation Wood / Copper (%)
Antenna 1 (proposed)	Impinj Monza R3	8.6	4.5	3.0	47.7 / 65.1
Antenna 5 (proposed)	Impinj Monza R3	6.3	1.45	0.5	77.0 / 92.1
Commercial tag A	Alien Higgs-2	7.2	5.5	1.9	23.6 / 73.6
Commercial tag B	NXP UCODE 8	6.5	5.0	2.5	23.1 / 61.5

Note: Wood values for Antennas 1 and 5 correspond to average measurements within the reported intervals. Degradation percentages are calculated with respect to the free-space read range.

Discussion:

The material-proximity measurements were conducted to emulate realistic deployment scenarios and to evaluate the robustness of the proposed tag antennas under dielectric and conductive loading conditions. In free-space operation at 866 MHz, Antenna 1 achieves a read range of 8.6 m, comparable to the selected commercial benchmarks (7.2 m for the ThinPropeller 2006 with Alien Higgs-2 IC and 6.5 m for the UCODE 8-based tag).

Under wood loading, all tags exhibit moderate degradation, which is consistent with dielectric loading effects. The presence of a dielectric layer modifies the effective permittivity surrounding the antenna, perturbs its electrical length, and alters the antenna–IC conjugate matching condition. As a result, the available power transferred to the chip decreases, leading to a reduced read range.

A significantly stronger degradation is observed under copper proximity. Conductive loading introduces severe detuning and reduces radiation efficiency due to induced surface currents and

 doi:10.20944/preprints202603.1222.v1

near-field confinement. These effects increase mismatch losses and raise the minimum activation threshold of the chip. In this critical scenario, Antenna 1 maintains a read range of approximately 3 m, which is comparable to the UCODE 8 benchmark (about 2.5 m) and higher than the ThinPropeller 2006 benchmark (about 1.9 m). This confirms that the proposed reference structure remains operational and competitive under conductive loading conditions.

In contrast, Antenna 5, although compact and well matched in free space, exhibits substantially higher sensitivity to nearby materials, reaching approximately 0.5 m under copper loading. This behavior reflects the inherent trade-off between miniaturization and environmental robustness. The stronger current confinement and increased quality factor associated with aggressive size reduction amplify detuning effects in the presence of external materials.

Beyond read-range analysis, the normalized radiation patterns demonstrate that the miniaturization process preserved the bidirectional angular distribution of the reference design. This characteristic remains advantageous for orientation robustness in practical tracking applications.

5. Conclusions

In this work, several UHF RFID tag antenna configurations were designed and experimentally evaluated, all derived from a common reference layout. Four initial structures were investigated by varying the IC placement within the coupling loop, demonstrating that chip positioning critically influences impedance matching, power sensitivity, and overall activation performance. Among the evaluated configurations, Antenna 1 exhibited the best performance, achieving a measured power sensitivity of −16.3 dBm at 866 MHz and a maximum read range of 8.6 m. This structure was selected as the baseline for miniaturization, leading to the development of Antenna 5. Despite its reduced physical dimensions, Antenna 5 maintained acceptable free-space performance, with a read range of 6.3 m and preserved bidirectional radiation characteristics. Material proximity tests under dielectric (wood) and conductive (copper) loading confirmed that the reference design maintains competitive robustness compared to commercially available RFID tags. The miniaturized version, while compact, exhibits increased sensitivity to conductive environments, highlighting the trade-off between size reduction and environmental stability. The comparative benchmark with commercial tags demonstrates that the proposed reference antenna achieves performance levels comparable to practical market solutions, particularly under conductive loading conditions. Overall, the results validate the effectiveness of IC-position optimization and controlled miniaturization in UHF RFID tag design, while clearly identifying the associated robustness limitations in aggressive compact configurations.

Acknowledgments: The authors gratefully acknowledge Professor Luca Catarinucci from the University of Salento for his guidance and for providing access to the EM-Tech Laboratory facilities. His support was essential for the fabrication and experimental validation of the proposed RFID tag structures.

References

1. Tariq, T.; Kuo, W.-C.; Mahmood, K.; et al. A lightweight authentication protocol for RFID-assisted supply chain management system. *IEEE Internet Things J.* **2024**, *12*, 12845–12852. https://doi.org/10.1109/JIOT.2024.3523390.
2. Khan, S.R.; Bernassau, A.L.; Desmulliez, M.P.Y. Passive and battery-free RFID-based wireless healthcare and medical devices: A review. *IEEE J. Radio Freq. Identif.* **2024**, *8*, 724–742. https://doi.org/10.1109/JRFID.2024.3451230.
3. Ali, W.; Zahid, M.; Shoaib, S.; et al. Performance analysis and design optimization of wearable RFID sensor-antenna system for healthcare applications. *IEEE Access* **2025**, *13*, 145540–145555. https://doi.org/10.1109/ACCESS.2025.3596519.
4. Gentili, G.B.; Dori, F.; Iadanza, E. Dual-frequency active RFID solution for tracking patients in a children's hospital: Design method, test procedure, risk analysis, and technical solution. *Proc. IEEE* **2010**, *98*, 1656–1662. https://doi.org/10.1109/JPROC.2010.2053330.
5. Xie, S.; Ma, C.; Feng, R.; et al. Wireless glucose sensing system based on dual-tag RFID technology. *IEEE Sens. J.* **2022**, *22*, 13632–13639. https://doi.org/10.1109/JSEN.2022.3179498.

 doi:10.20944/preprints202603.1222.v1

6. Barba, A.B.; Panunzio, N.; Amendola, S.; et al. A multi-antenna RAIN RFID sensing architecture for pharmaceutical climatic chambers. *IEEE J. Radio Freq. Identif.* **2025**, *9*, 517–526. https://doi.org/10.1109/JRFID.2025.3587760.
7. Zhang, X.; Zhang, X. Application of radio frequency identification technology in maintenance tracking of aircraft electromechanical equipment. In *Proceedings of the 2024 International Conference on Electrical Drives, Power Electronics & Engineering (EDPEE)*, 2024; pp. 580–585. https://doi.org/10.1109/EDPEE61724.2024.00114.
8. Xiao, L.; Yin, Y.; Wu, X.N.; Wang, J.W. A large-scale RF-based indoor localization system using low-complexity Gaussian filter and improved Bayesian inference. *Radioengineering* **2013**, *22*, 371–380.
9. Occhiuzzi, C.; Amendola, S.; Nappi, S.; et al. RFID technology for Industry 4.0: Architectures and challenges. In *Proceedings of the 2019 IEEE International Conference on RFID Technology and Applications (RFID-TA)*, 2019; pp. 181–186. https://doi.org/10.1109/RFID-TA.2019.8892049.
10. Komma, P.; Vogelbruch, M.; Jung, M. Digital twins in industrial automation: A closer look on RFID read/write components for virtual commissioning. In *Proceedings of the 2024 IEEE 22nd International Conference on Industrial Informatics (INDIN)*, 2024; pp. 1–8. https://doi.org/10.1109/INDIN58382.2024.10774431.
11. Nappi, S.; Amendola, S.; Ramacciotti, M.; et al. UHF RFID system for the predictive maintenance of a filter press: A real use case. In *Proceedings of the 6th International Conference on Smart and Sustainable Technologies (SpliTech)*, 2021; pp. 1–4. https://doi.org/10.23919/SpliTech52315.2021.9566441.
12. Othmani, H.; Beldi, S.; Azizi, M.K. Design of an SHF RFID reader antenna for access control and security systems. In *Proceedings of the 2024 IEEE International Conference on Advanced Systems and Emergent Technologies (IC_ASET)*, 2024; pp. 1–5. https://doi.org/10.1109/IC_ASET61847.2024.10596171.
13. Shimizu, K.; Wang, S.; Kai, H.; et al. A lightweight and secure one-time RFID authentication protocol based on SAS-L2. In *Proceedings of the 2024 IEEE International Conference on Consumer Electronics-Asia (ICCE-Asia)*, 2024; pp. 1–4. https://doi.org/10.1109/ICCE-Asia63397.2024.10773800.
14. Panda, J.R.; Saladi, A.S.R.; Kshetrimayum, R.S. A compact printed monopole antenna for dual-band RFID and WLAN applications. *Radioengineering* **2011**, *20*, 464–467.
15. Riaz, M.A.; Abdullah, Y.; Shahid, H.; et al. Novel butterfly slot based chipless RFID tag. *Radioengineering* **2018**, *27*, 776–783. https://doi.org/10.13164/re.2018.0776.
16. Chaffai, K.M.; Berenguer, R.; Rezola, A.; et al. Exploring dual-frequency implementation for semi-passive RFID tags. In *Proceedings of the 39th Conference on Design of Circuits and Integrated Systems (DCIS)*, 2024; pp. 1–6. https://doi.org/10.1109/DCIS62603.2024.10769162.
17. Nath, B.; Reynolds, F.; Want, R. RFID technology and applications. *IEEE Pervasive Comput.* **2006**, *5*, 22–24. https://doi.org/10.1109/MPRV.2006.13.
18. Siakavara, K.; Goudos, S.; Theopoulos, A.; Sahalos, J.N. Passive UHF RFID tags with specific printed antennas for dielectric and metallic objects applications. *Radioengineering* **2017**, *26*, 735–745. https://doi.org/10.13164/re.2017.0735.
19. Räsänen, M.; Holopainen, J.; Bergman, J.; et al. Small on-metal passive UHF RFID transponders with long read ranges. In *Proceedings of the 18th European Conference on Antennas and Propagation (EuCAP)*, 2024; pp. 1–4. https://doi.org/10.23919/EuCAP60739.2024.10501750.
20. Bouazza, H.; Lazaro, A.; Bouya, M.; Hadjoudja, A. A planar dual-band UHF RFID tag for metallic items. *Radioengineering* **2020**, *29*, 504–511. https://doi.org/10.13164/re.2020.0504.
21. Marrocco, G. The art of UHF RFID antenna design: Impedance-matching and size-reduction techniques. *IEEE Antennas Propag. Mag.* **2008**, *50*, 66–79. https://doi.org/10.1109/MAP.2008.4494504.
22. Nikitin, P.V.; Rao, K.V.S.; Lam, S.F.; et al. Power reflection coefficient analysis for complex impedances in RFID tag design. *IEEE Trans. Microw. Theory Tech.* **2005**, *53*, 2721–2725. https://doi.org/10.1109/TMTT.2005.854191.
23. Chen, R.; Yang, S.; Penty, R.V.; Crisp, M. UHF RFID reader sensitivity requirements due to poor tag matching. In *Proceedings of the 12th IEEE International Conference on RFID Technology and Applications (RFID-TA)*, 2022; pp. 90–93. https://doi.org/10.1109/RFID-TA54958.2022.9924099.
24. Dobrykh, D.; Yusupov, I.; Slobozhanyuk, A.; et al. Compact long-range ceramic RFID tag for on-metal and non-metal applications. In *Proceedings of the 12th IEEE International Conference on RFID Technology and Applications (RFID-TA)*, 2022; pp. 94–97. https://doi.org/10.1109/RFID-TA54958.2022.9923978.
25. Tan, J.-I.; Lee, Y.-H.; Lim, E.-H. Design of a compact on-metal RFID tag with a pair of planar inverted-L antennas (PILAs). In *Proceedings of the 12th IEEE International Conference on RFID Technology and Applications (RFID-TA)*, 2022; pp. 126–127. https://doi.org/10.1109/RFID-TA54958.2022.9924083.

 doi:10.20944/preprints202603.1222.v1

26. Franchina, V.; Michel, A.; Nepa, P.; Salvatore, A. Compact in-metal UHF RFID tag for manufactured metallic components. In *Proceedings of the 3rd International Conference on Smart and Sustainable Technologies (SpliTech)*, 2018; pp. 1–5.
27. Nabavi, S.; Anabestani, H.; Bhadra, S. A printed paper-based RFID tag for wireless humidity sensing. In *Proceedings of the IEEE Sensors Conference*, 2022; pp. 1–4. https://doi.org/10.1109/SENSORS52175.2022.9967219.
28. Wang, Y.; Liu, J.; Xie, L.; Wen, G. An ultra-low-power oscillator with temperature and process compensation for UHF RFID transponder. *Radioengineering* **2013**, *22*, 505–510.
29. Kanjilal, R.; Kucuk, M.F.; Uysal, I. Human activity recognition: A review of RFID and wearable sensor technologies powered by AI. *IEEE J. Radio Freq. Identif.* **2025**, *9*, 180–199. https://doi.org/10.1109/JRFID.2025.3561345.
30. Renuka, N.; Chin, N.N.; Ismail, W. Embedded RFID tracking system for hospital application using WSN platform. In *Proceedings of the IEEE International Conference on RFID Technologies and Applications (RFID-TA)*, 2013; pp. 1–5. https://doi.org/10.1109/RFID-TA.2013.6694539.
31. Franchina, V.; Ria, A.; Michel, A.; et al. A compact UHF RFID ceramic tag for high-temperature applications. In *Proceedings of the IEEE International Conference on RFID Technology and Applications (RFID-TA)*, 2019; pp. 480–483. https://doi.org/10.1109/RFID-TA.2019.8892217.
32. Albrecht, J.; Dudek, R.; Auersperg, J.; et al. Thermal and mechanical behaviour of an RFID based smart system embedded in a transmission belt determined by FEM simulations for Industry 4.0 applications. In *Proceedings of the 16th International Conference on Thermal, Mechanical and Multi-Physics Simulation and Experiments in Microelectronics and Microsystems*, 2015; pp. 1–5. https://doi.org/10.1109/EuroSimE.2015.7103152.
33. Cummins, D.; Claucherty, E.; Nowaczyk, J.; et al. A practical assessment of integrating RFID into over-the-counter liquid suspension supply chains. In *Proceedings of the IEEE International Conference on RFID Technology and Applications (RFID-TA)*, 2024; pp. 13–16. https://doi.org/10.1109/RFID-TA64374.2024.10965156.
34. Yeh, C.-H.; Ho, P.-S.; Lin, C.-W.; Sim, C.-Y.-D. Circularly polarized UHF RFID tag antenna with capacitive loading technique. In *Proceedings of the 5th IEEE Asia-Pacific Conference on Antennas and Propagation (APCAP)*, 2016; pp. 451–452. https://doi.org/10.1109/APCAP.2016.7843286.
35. Loo, C.-H.; Elmahgoub, K.; Yang, F.; et al. Chip impedance matching for UHF RFID tag antenna design. *Prog. Electromagn. Res.* **2008**, *81*, 359–370.
36. Ripin, N.; Rahim, M.K.A.; Lim, E.-H.; et al. Metal-tolerant UHF RFID tag antenna with a comb-shaped design. In *Proceedings of the IEEE Asia-Pacific Conference on Applied Electromagnetics (APACE)*, 2024; pp. 120–123. https://doi.org/10.1109/APACE62360.2024.10877337.
37. El Ahmar, L.; Errkik, A.; Zbitou, J.; et al. A compact meander flexible UHF tag for industrial applications. *e-Prime Adv. Electr. Eng. Electron. Energy* **2024**, *7*, 100402. https://doi.org/10.1016/j.prime.2023.100402.
38. Impinj Inc. *Impinj Monza R3 Datasheet*; 2025. Available online: https://www.impinj.com/fr/products/tag-chips (accessed on 18 August 2025).